Geophys. J. Int. (1999) **136,** 695–704

A seismic cross-section through the east European continent

Everhard Muyzert,* Hanneke Paulssen and Roel Snieder
Department of Geophysics, Utrecht University, PO Box 80021, 3508 *TA, Utrecht, the Netherlands*

Accepted 1998 October 2. Received 1998 October 2; in original form 1997 December 10

SUMMARY

A 2-D profile for the shear wave velocity and anisotropy between Egypt and Spitsbergen is presented. The profile is constructed using fundamental- and higher-mode Love and Rayleigh waves recorded by stations of the NARS-DEEP, IRIS and GEOFON networks. The surface wave data have been inverted for shear velocity and anisotropy using a waveform inversion. In the eastern Mediterranean lithosphere we observe a large difference (7 per cent) between *SH* and *SV* velocities. We interpret this anomaly as an anisotropic oceanic lithosphere beneath the eastern Mediterranean, an interpretation which is consistent with tectonic reconstructions of the region. The east European continent is imaged as a high-velocity body whose thickness increases with the estimated age of the lithosphere. The continental root of the Ukrainian and Baltic shields and east European platform extends to a depth of 200 km. This is in contrast to the surrounding younger continental regions which appear to be less than 100 km thick. We further studied the structure of the continental lithosphere by investigating a possible relation between seismic velocities and tectonic age. Both a logarithmic and a square root relation have been fitted to the average seismic velocities in each tectonic region. The data slightly favour a logarithmic relation but a square root relation cannot be excluded.

Key words: anisotropy, continental evolution, eastern Europe, seismic tomography, surface waves.

1 INTRODUCTION

The east European continent consists of a variety of tectonic units ranging from possible oceanic plates (eastern Mediterranean) to the Archaean Ukrainian and Baltic shields. The crustal structure of the region is well studied, e.g. Pavlenkova (1996), but the structure of the lithosphere is poorly known. Considerable heterogeneities in the east European lithosphere have been observed down to a depth of 300 km using *P* wave travel-time data (e.g. Husebye & Hovland 1982; Grad, Kryzanowska & Pirhonen 1995). Recent higher-mode surface wave studies have mapped the transition from the Phanerozoic western European towards the Precambrian east European platform along the Tornquist–Teisseyre zone and revealed a difference in seismic velocities down to 300 km depth (Zielhuis & Nolet 1994; Marquering & Snieder 1996). However, high-resolution tomographic studies of the east European platform have not yet been performed due to the lack of digital broad-band seismic stations.

Seismological data put important constraints on models of the evolution of the continental lithosphere (Jordan 1981; Durrheim & Mooney 1994). The basic idea in such theories is that the chemical content and the thickness of the continents vary with lithospheric age due to the increased mantle temperature in the Archaean. One such observation is the increase of crustal thickness with lithospheric age (Meissner 1986; Durrheim & Mooney 1994). Other important seismological observables are the thickness of the continental lithosphere and changes in velocities due to temperature and chemical variations in the continental lithosphere. The poor knowledge of the continental lithosphere is in contrast to the knowledge of the oceanic lithosphere (Sclater, Jaupert & Galson 1980). Heat flow and bathymetry in the oceanic lithosphere older than 80 Ma follow a logarithmic relation instead of a square root relation. Such a logarithmic relation is predicted by a cooling model of a 125 km thick lithospheric plate.

In this study we present a 2-D model for shear velocity and anisotropy from Egypt to Spitsbergen. This profile connects three earthquakes in the eastern Mediterranean and Spitsbergen with seven stations in the region. The locations of these stations allow us to determine the seismic velocities of

* Now at: Schlumberger Cambridge Research, High Cross, Madingley Road, Cambridge CB3 0EL, UK.

several tectonic units such as the eastern Mediterranean Sea, the east European platform and the Baltic shield; see Fig. 1(a). The main data sources are four stations of the NARS-DEEP network that have been installed along a line from Odessa to St Petersburg, thus covering the east European platform; see Snieder & Paulssen (1993). In addition we use data from several recently installed IRIS and GEOFON stations in the region.

The data set, which consists of fundamental- and higher-mode Love and Rayleigh waves, is inverted using a partitioned waveform inversion analogous to Nolet (1990). Such a waveform inversion has the advantage over dispersion measurements in that it is not necessary to identify the modes in the seismogram. Interference of higher modes with each other and of higher modes with the fundamental mode is implicitly taken into account and does not bias the inversion. We illustrate the lateral and depth resolution of the waveform inversion by a synthetic test. It is well known that the inversion of Love and Rayleigh waves can lead to different *SH* and *SV* models, e.g. Babuska & Cara (1991). As a Love–Rayleigh discrepancy is present in our data set we include anisotropy in the inversion.

We discuss the lateral variation and the depth extent of the anomalies in the model and relate these to the tectonic history of the regions. The seismic velocities and anisotropy of the eastern Mediterranean lithosphere are strikingly different from those in the continent and therefore we discuss this

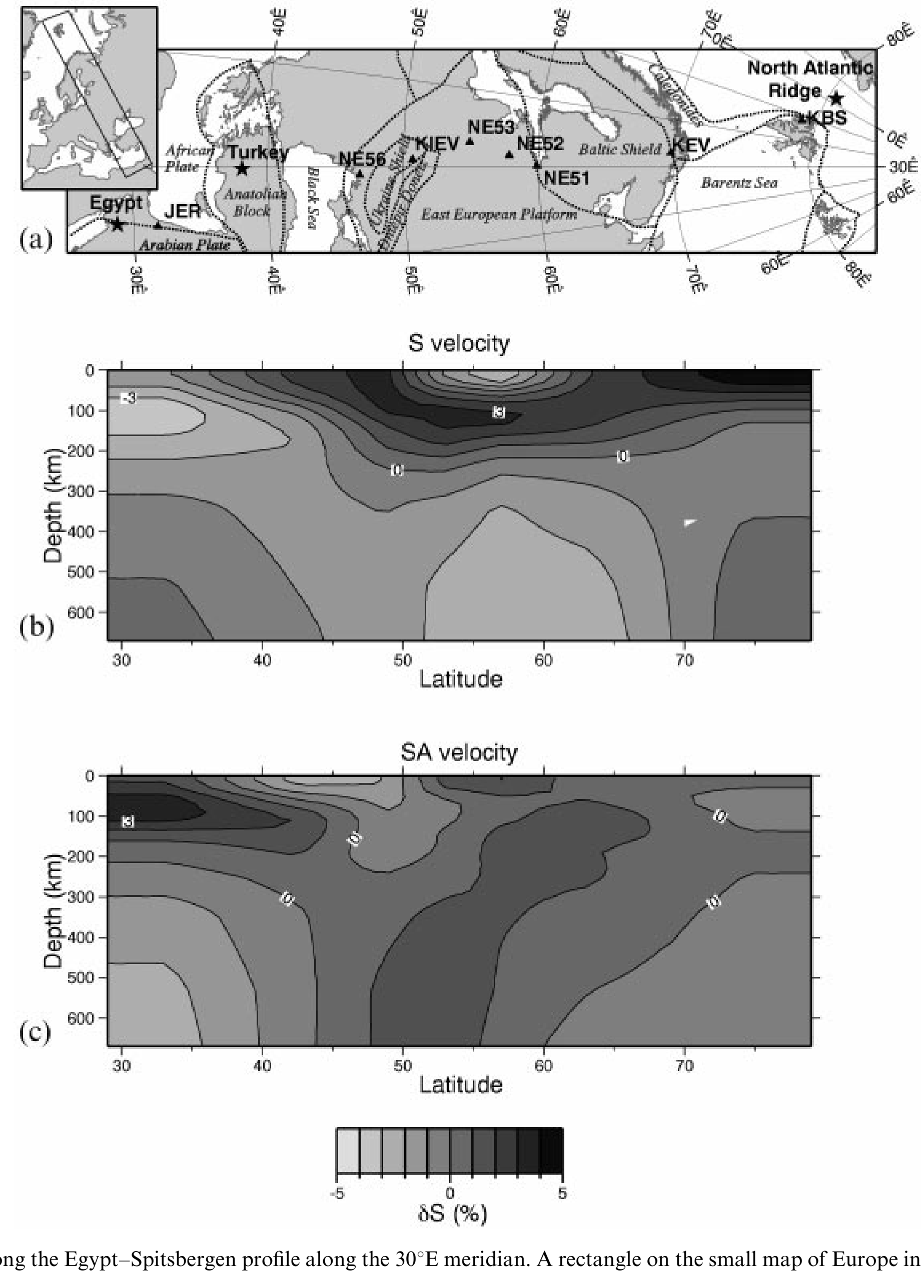

Figure 1. (a) Map along the Egypt–Spitsbergen profile along the 30°E meridian. A rectangle on the small map of Europe in the upper left corner of the figure indicates the location of the profile. Shown on the main map are seismic stations (triangles), event locations (stars) and the tectonic regions after Zonenshain *et al.* (1990). (b) *S*-velocity model of the lithosphere and mantle between Egypt and Spitsbergen. (c) Apparent anisotropy *SA* model for the same region.

region in a separate section. In the last section we investigate a possible relation between seismic velocities in the continental lithosphere and tectonic age.

2 DATA

We have collected data from three strong earthquakes. Two events took place in the eastern Mediterranean: Turkey, 1995 October 1, $M_w=6.0$ and Egypt, 1995 November 22, $M_w=7.2$. The third event is located along the northern Atlantic ridge, 1996 May 14, $M_w=5.7$. The epicentres of these earthquakes are located on a great circle connecting eight seismic stations in eastern Europe and the eastern Mediterranean for which data were available; see Fig. 1(a) and Table 1. Among them are the NARS-DEEP stations NE51 (St. Petersburg, Russia), NE52 (Pskov, Russia), NE53 (Naroch, Belarus) and NE56 (Odessa, Ukraine). Together with the NARS-DEEP data we use registrations from the IRIS stations KEV (Kevo, Finland), KBS (Kingsbay, Spitsbergen) and KIEV (Kiev, Ukraine). In addition we include recordings of the northern Atlantic ridge event by the GEOFON station JER (Jericho, Israel). Data from other stations and events in the region were either of poor quality or not available.

The seismograms have been corrected for instrument response, and after visual inspection for noise, 14 transverse-component seismograms and 16 vertical-component seismograms were selected for surface wave analysis. The vertical-component seismograms show strong fundamental and higher-mode Rayleigh waves together with *S* and *SS* phases. Due to the shallow source depth of the events, the transverse-component seismograms contain mainly strong fundamental-mode Love waves and poorly developed higher modes and body wave phases. All waveforms have been checked for sensitivity to uncertainties in the source parameters; see Muyzert & Snieder (1996).

3 WAVEFORM INVERSION

The seismic velocities between the stations and events have been determined by a partitioned waveform inversion similar to the method developed by Nolet (1990). This is a two-step method. First, each seismogram is inverted for the path-averaged shear velocity structure. Both Love and Rayleigh waves have been inverted from the direct *S* wave up to the fundamental-mode arrival. In this approach, the body wave phases *S* and *SS* are modelled by the summation of many higher modes. In the second step all path-averaged velocity functions are combined and inverted for the lateral velocity variations between the stations. In this step anisotropy has been introduced in the model as isotropic models could not fit both the Love and the Rayleigh wave data equally well.

Table 1. Station locations and epicentres of earthquakes.

Station	Latitude (°N)	Longitude (°E)
JER	31.72	35.18
NE51	59.88	34.82
NE52	57.82	28.39
NE53	54.90	26.79
NE56	46.78	30.88
KEV	69.75	27.00
KBS	78.92	11.92
KIEV	50.69	29.21
Egypt event	28.81	34.86
Turkey event	38.10	30.18
Northern Atlantic Ridge event	80.78	−2.27

In the first step of the inversion procedure the seismograms are filtered in both time and frequency in order to separate phases. The fundamental-mode data has large frequency-dependent amplitude variations and is therefore filtered into two different windows with frequencies between 0.01 and 0.03 Hz and 0.005 and 0.01 Hz. In addition, two higher-mode windows have been defined, one around the *S*, the other around the *SS* phases, both at frequencies between 0.016 and 0.05 Hz. At epicentral distances smaller than 2000 km the *S* and *SS* phases could not be separated and a window containing both phases has been used. For Love waves at shorter distances a window is chosen that contains the *SS* phase and the fundamental mode.

Each seismogram is separately inverted using the objective function defined by

$$F(\mathbf{m})=\int[D(t)-S(t,\mathbf{m})]^2\,dt+\gamma_{\mathbf{m}} \tag{1}$$

(see Nolet 1990). In eq. (1), $D(t)$ and $S(t,\mathbf{m})$ are the filtered data and synthetic seismogram computed for the path-averaged velocity model $\mathbf{m}$. The term $\gamma_{\mathbf{m}}$ denotes a regularization term which is a two-point smoothing operator that penalizes the vertical gradient of the model. Eq. (1) is minimized using the conjugate gradient method. To prevent the inversion from being trapped in local minima, long-period fundamental modes are inverted first. In subsequent iterations the depth resolution is increased by adding the higher-mode windows and higher frequencies to the objective function.

The model parameters of the waveform inversion are the relative perturbations in the horizontal shear velocity $SH(z)$ for the Love wave data and the vertical shear velocity $SV(z)$ for the Rayleigh wave data. The shear velocity model is parametrized in nine layers with increasing thickness. The top layer is the crustal layer with a thickness of 40 km. The bottom layer is defined from 670 km depth to the core–mantle boundary. The starting model for the inversion has a Moho depth of 40 km and a constant shear velocity of 4.5 km s^{-1} between 40 and 220 km. Below 220 km depth the PREM model (Dziewonski & Anderson 1981) is used. ISC locations and Harvard source mechanisms have been used for the modelling of the waveform.

A Love–Rayleigh discrepancy can occur in the final model because the Love and Rayleigh waves were separately inverted for the *S* velocity. Mitchel (1984) showed that the Love–Rayleigh discrepancy present in dispersion data from the central United States could be explained by isotropic models with thin layers. We have not taken such an approach as it would limit our data set. This requires a joint waveform inversion of both Love and Rayleigh data from all common source–receiver paths. Another cause for a Love–Rayleigh discrepancy is lateral variations in the crustal structure; see Levshin & Ratnikova (1984). We take these variations into account by applying on each seismogram a crustal correction computed for the CRUST5.1 model (Mooney, Laske & Masters 1998). The CRUST5.1 model reflects the major variations in the crust as it consists of 5° × 5° cells. For each of these cells *P* and *S* velocities and densities are given, collected from a large number of crustal studies including eastern

Europe. Along the profile we have computed the difference between the phase velocity in the starting model and the local phase velocity in each cell of the CRUST5.1 model. The crustal correction is taken as the sum of these local phase velocity perturbations from the cells along the source–receiver path. Thus the seismograms include the effect of the variation in crustal structure, Moho depth and water layer on a large scale. The application of the crustal correction has resulted in a smaller difference between SH and SV velocities in the layer directly below the Moho in the final model. With improved crustal models and modelling techniques this difference might become even smaller.

In the second step of the inversion the path-averaged velocity perturbations are inverted for the interstation velocities. In this inversion the cell boundaries have been defined by the latitudes of the earthquakes and stations. The only exception is on the east European platform where a cell ranging from NE53 to NE51 has been defined, as tests indicated that the cell NE52–NE51 could not be resolved due to its small horizontal length.

As we will show later, a Love–Rayleigh discrepancy is present in the path-averaged velocity functions obtained in the waveform inversion. We include anisotropy in the second inversion where the path averaged velocity functions of both the Love and Rayleigh wave data are combined. A commonly used parameter set for the inversion of surface waves is SV and $\xi=(SH/SV)^2$. This parameter set is useful for the inversion of phase velocities but not for the path-averaged velocity functions, as it results in a non-linear inversion for $SH(z)$. Instead we define the average shear velocity $S=(SH+SV)/2$ and the apparent shear wave anisotropy $SA=(SH-SV)/2$. The relation between the path-averaged velocity functions and S and SA is linear. Another advantage of this parameter set is that the S velocity has only a weak dependence on SA while the estimate for SV has an implicit trade-off with ξ. Hereinafter the symbols S and SA refer to the relative variations in these parameters.

The inversion of the path-averaged velocity function for S and SA is linear and regularized by both smoothing and norm damping of the model. This results in the following set of linear equations that is solved in the least-squares sense (see Paige & Saunders 1982):

$$\begin{bmatrix} \mathbf{A}_1 & 0 \\ \eta\mathbf{G} & 0 \\ 0 & \mathbf{A}_2 \\ 0 & \eta\mathbf{G} \\ 0 & \mu\mathbf{I} \end{bmatrix} \begin{bmatrix} S \\ SA \end{bmatrix} = \begin{bmatrix} SH+SV \\ 0 \\ SH-SV \\ 0 \\ 0 \end{bmatrix}. \tag{2}$$

In eq. (2) the elements of the matrices $\mathbf{A}_1$ and $\mathbf{A}_2$ are the distances each seismic wave has travelled through each cell. $\mathbf{G}$ is the operator that smooths the horizontal and vertical gradient of S and SA and whose importance can be varied by adjusting the parameter η. The amount of apparent anisotropy SA can be minimized by adjusting the damping parameter μ which is multiplied by the identity matrix $\mathbf{I}$.

We illustrate the resolution of the inversion by a checkerboard synthetic test. The input model for the checkerboard test is an alternating pattern with 10 per cent variation in S and SA; see Fig. 2(a). In Fig. 2(a) the true amplitude of each cell has been plotted in the midpoint of each cell. Between the cell midpoints linear interpolation has been applied in order to obtain a smooth image. The choice of the S perturbation is important as we compute the synthetic seismograms for the corresponding SH and SV models. When we define S similar to SA the perturbation in SV is zero throughout the model and the inversion of the Rayleigh waves becomes trivial. We have therefore shifted the pattern of the S perturbations to 0 and 10 per cent which leads to a constant SV perturbation of 5 per cent.

The synthetic seismograms have been computed for the path-averaged velocity functions of the input model and are inverted using the same inversion procedure as applied to the real data. The retrieved S and SA models are shown in Figs 2(b) and (c) where a constant value of 5 per cent is subtracted from the S velocity for visual display. These figures show that the S and SA velocities are equally well resolved. The resolution is good at the top and the centre of the model. At depths larger than 400 km in the southern and the northern part the amplitude of S and SA is poorly recovered. Random noise and uncertainties in the excitation will influence the results of this resolution test. However, in the real data these errors are small as the data have been selected for a high signal-to-noise ratio and small sensitivity to uncertainties in the source mechanism.

4 THE MODEL

A preferred model has been selected on the basis of a trade-off analysis between model roughness and data misfit; see Fig. 3. We have tested a large number of combinations of the regularization parameters η and μ in the range 10–2000. The model roughness is defined as the sum of the gradient smoothing and the anisotropy damping. The data misfit is the sum of the misfit between data and synthetic waveforms computed for the corresponding velocity model and is given by the first term on the right-hand side of eq. (1). The minimum-norm model, which is the point close to the origin on the trade-off curve, is a logical but subjective choice which depends on the scaling of the axis, the relative importance of the smoothness of the model, and the amount of anisotropy. After visual checks of the waveforms computed for the range of tested models we have selected a slightly rougher model which has stronger gradients in S but less apparent anisotropy SA than the minimum-norm model. The preferred model is computed for $\eta=250$ and $\mu=500$ and is indicated by the star in Fig. 3.

The preferred model for the S velocity and the apparent anisotropy SA is shown in Figs 1(b) and (c). The S velocity model shows a clear signature of the European continent with 7 per cent lateral variations in lithosphere between the crust and 200 km depth. At the southern boundary of the model, under the eastern Mediterranean, we find low S velocities in the lithosphere. The mantle under the lithosphere in this region is poorly resolved. Under Turkey and the Black Sea we find a high-velocity zone overlaying the asthenosphere which has a 5 per cent lower S velocity. Velocities increase even further under the east European platform, and the Ukrainian and Baltic shield where the thickness of the high-velocity layer increases to 200 km. Under the east European platform at a depth larger than 300 km low velocities are observed. In the Barents sea region the thickness of this high-velocity layer is approximately 100 km. The model of the apparent anisotropy SA is rather different. Under the eastern Mediterranean high SA values (3.5 per cent) are found in a well-defined region

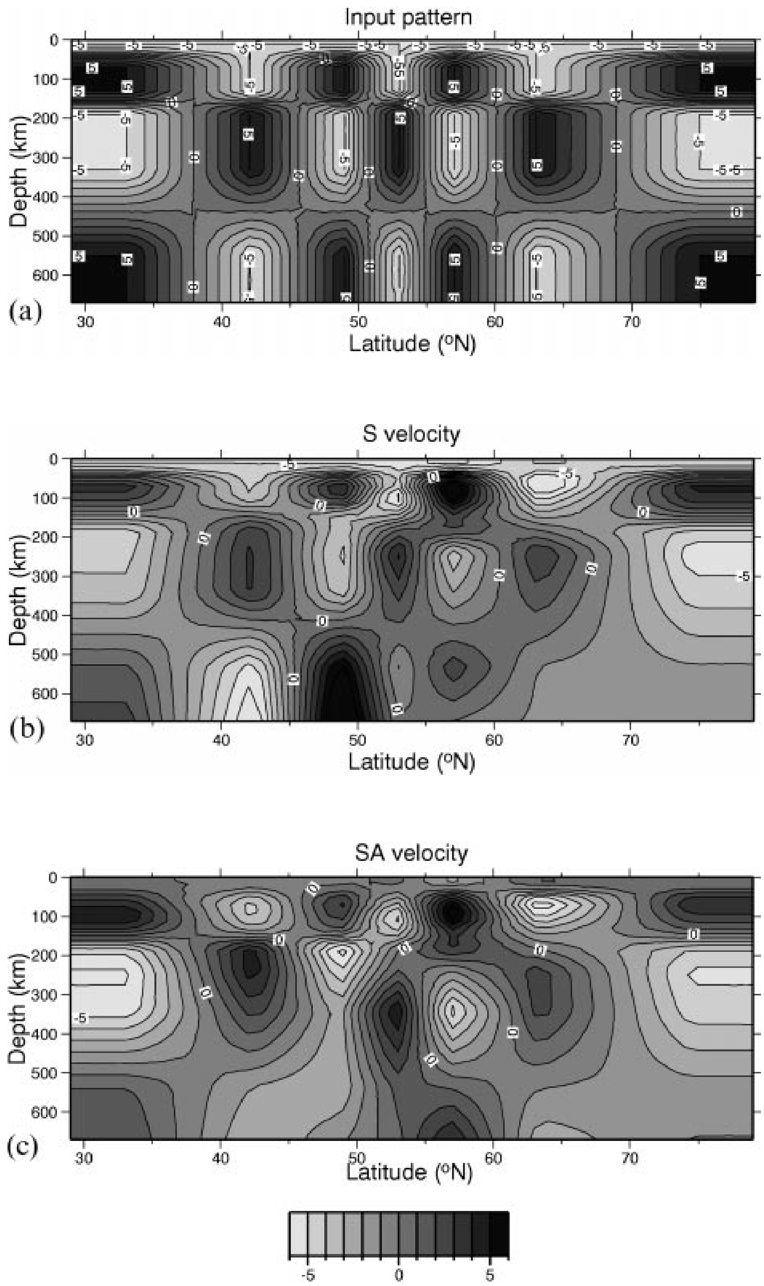

Figure 2. (a) Pattern of checkerboard synthetic test for the model presented in Fig. 1. (b) Recovered *S*-velocity model. Input model has perturbations of (0–10 per cent) from which 5 per cent has been subtracted for visual display. (c) Recovered SA velocity model. Input pattern has perturbation of (-5, -5) per cent.

at 100 km depth. Under the continent a broad region with increased *SA* values ($SA < 1.5$ per cent) can be identified. The shape of this structure does not correlate with variations in the *S* velocity model.

The model fits the data very well. Fig. 4(a) shows the waveform fits for the Rayleigh waves of the Egypt event. Both the fundamental modes and the *S* and *SS* phases have good fits. Only the relative amplitude of these phases shows a poorer fit. This is probably caused by variations in attenuation which are not accounted for. A typical fit to the Love wave data is shown in Fig. 4(b).

It is important to investigate whether the apparent anisotropy *SA* is required in the model. We have therefore inverted the data set only for the *S* velocity and performed a trade-off analysis; the results are indicated by the plus symbols (+) in Fig. 3. The model roughness is in general smaller than that for the anisotropic inversion because now the model roughness of the *SA* is not included. The data misfit of even the best-fitting isotropic model is significantly worse than for the models with apparent anisotropy. The preferred isotropic *S* model is remarkably similar to the model with *SA* included (compare Figs 1b and 5). From this we can conclude that there is little trade-off between the *S* and *SA* velocities.

The presence of apparent anisotropy is clearly visible in the data. In Fig. 6 we show data for the northern Atlantic ridge event together with synthetics for the *S* velocity of the

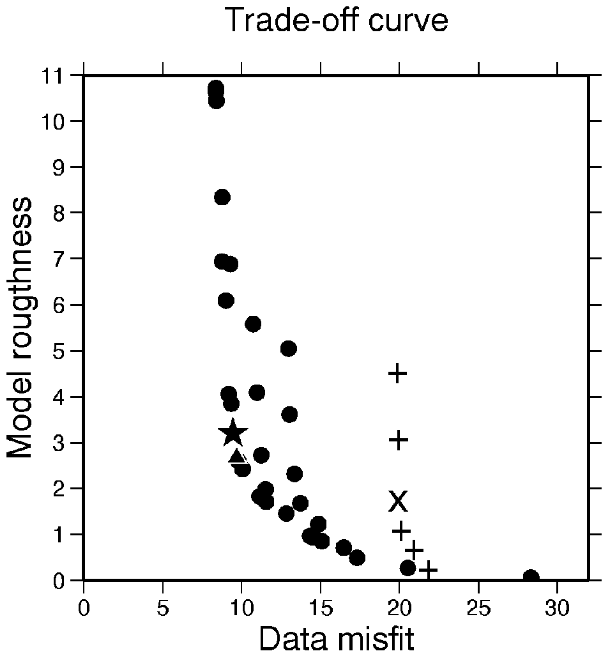

Figure 3. Trade-off curve for model roughness versus data misfit. Circles represent tested anisotropic models. The triangle indicates the minimum norm model. The preferred model is indicated by the star. Plus signs indicate the isotropic models of which the preferred model is marked by the cross.

isotropic model displayed in Fig. 5. Fundamental-mode Love and Rayleigh waves recorded at station KIEV fit well with synthetics computed for the isotropic model, which means that there is only a little *SA* in the lithosphere between Spitsbergen and KIEV. Seismograms recorded 20° further south in JER, however, show a poor fit to the synthetics for the isotropic *S* model. Larger *SH* velocities and smaller *SV* velocities resulting in significant apparent anisotropy *SA* are required to explain the data. We have also observed this phenomenon for seismograms of the Egypt and Turkey events. Thus we have a stable observation of apparent anisotropy *SA*.

5 THE EASTERN MEDITERRANEAN

The observed apparent anisotropy *SA* in the eastern Mediterranean could be due to inexact modelling of the crustal structure. Levshin & Ratinkova (1984) have explained the 2 per cent difference in *SV* and *SH* velocities between 20 and 220 km depth in the PREM model by lateral variations in the Moho depth. For our model we have computed a crustal correction using the $5^\circ \times 5^\circ$ crustal model CRUST5.1 (Mooney *et al.* 1998). This model shows that the crustal structure in the eastern Mediterranean is very different from the continent with different Moho depth (26 km versus 40 km), thickness of the sedimentary layers and the presence of a water layer. The crustal correction for the short-period fundamental Rayleigh wave ($T < 20$ s) in the eastern Mediterranean is larger than 10 per cent. However, at these periods the Rayleigh

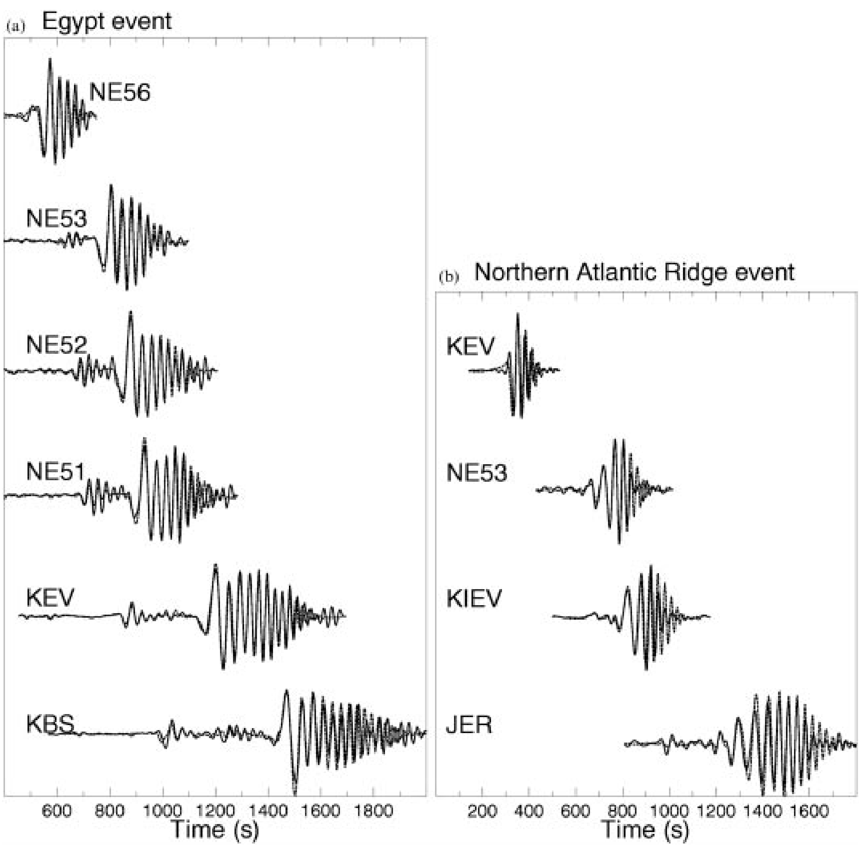

Figure 4. (a) Waveform fit of the Rayleigh waves from the Egypt event, filtered between periods $25 < T < 100$ s. The solid line represents the data; the dashed line corresponds to the synthetic seismograms. (b) Waveform fit for Love waves of the northern Atlantic ridge event.

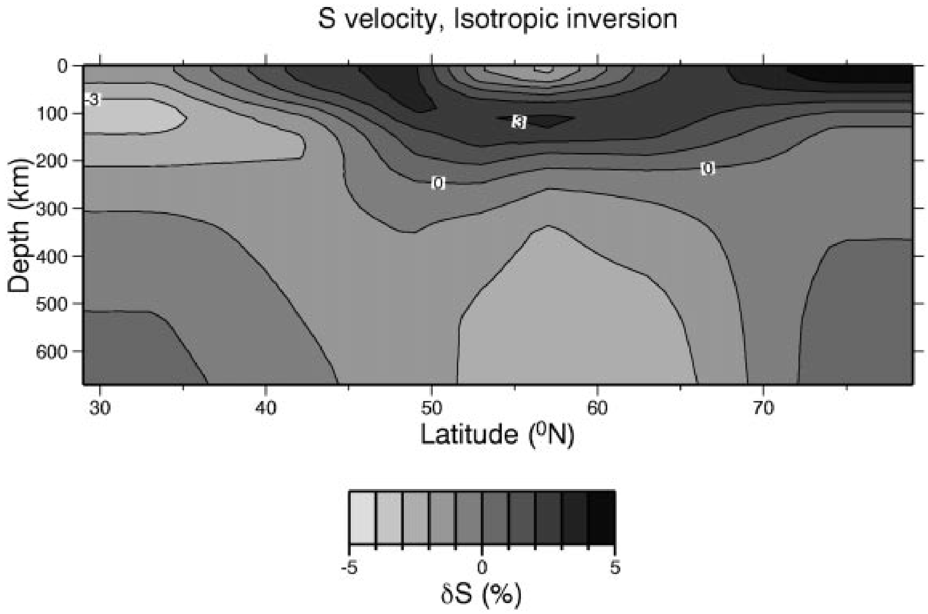

Figure 5. *S* velocity model obtained by isotropic inversion.

wave only samples the crust. The size of the crustal correction quickly decreases for increasing period as the surface wave penetrates deeper into the mantle. At a period of 40 s the crustal correction is only 2 per cent and is not sufficient to explain the observed Love–Rayleigh discrepancy. Because of the magnitude of the Love–Rayleigh discrepancy (7 per cent), our preferred interpretation of this anomaly is the presence of anisotropy in the lithosphere.

The interpretation of anisotropy in the eastern Mediterranean is supported by tectonic reconstructions. Dercourt *et al.* (1986) proposed the presence of an oceanic plate in the eastern Mediterranean that has been subducted under Eurasia during the closure of the Tethys Ocean. This hypothesis of an oceanic lithosphere is based on tectonic reconstructions and the only direct evidence for it comes from seismic studies. Oceanic crust has been identified on seismic profiles shot in the Ionian Sea (20°E) (de Voogd *et al.* 1992). Along our profile at 30°E, however, neither surface wave nor seismic reflection studies can discriminate between oceanic crust and thinned continental crust (Cloetingh, Nolet & Wortel 1980; de Voogd *et al.* 1992). Models for oceanic lithosphere younger than 100 Ma show a 6 per cent anisotropy down to 160 km, *SV* velocities between 120 and 200 km of 4.3 km s^{-1} and the presence of a shallow high-velocity lid (depth < 100 km); see Nishimura & Forsyth (1989). Our velocity model for the eastern Mediterranean is in agreement with these models for the oceanic lithosphere and therefore with the reconstructions of Dercourt *et al.* (1986).

6 EAST EUROPEAN CONTINENT

The geological history of the east European continent is very different from that of the eastern Mediterranean. The southern part of the Eurasian continent consists of different tectonic blocks, such as the Anatolian block and the Black Sea region,

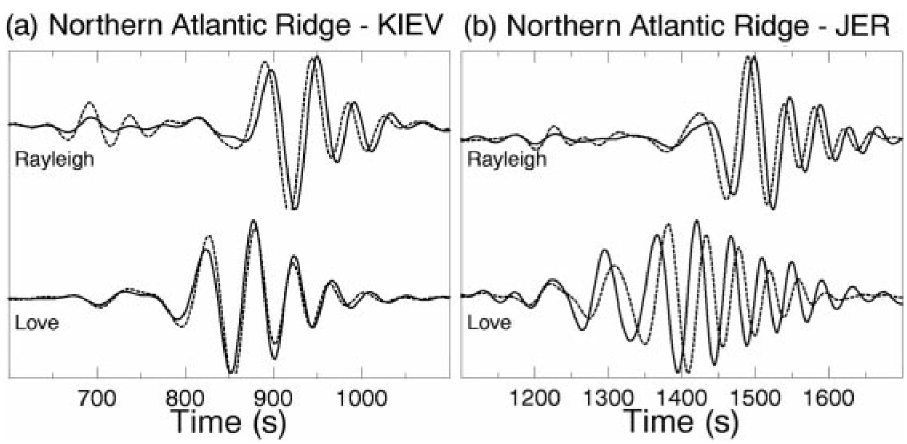

Figure 6. (a) Waveform fit to the isotropic model for Love and Rayleigh waves for the northern Atlantic ridge event recorded in KIEV. Synthetics (dashed line) have been computed for the isotropic *S* model shown in Fig. 5. Seismograms are low-pass filtered at $T=50$ s. (b) Waveform fit for station JER.

which were pressed on to the east European platform (EEP) and Ukrainian shield in the late Cretaceous (Dercourt *et al.* 1986). This region with tectonic activity, which has probably caused thermal and chemical anomalies, shows in our model as a thin high-velocity lid overlying a pronounced low-velocity zone with little apparent anisotropy. A similar but less pronounced velocity structure is observed under the Baltic Sea microplate in which the most recent tectonic activity is the collision with the Baltic shield and the Caledonides 600 Myr ago. The high-velocity anomaly associated with the continent extends to a depth of 100 km.

The EEP between stations NE53 and NE51 is early Proterozoic; see Zonenshain, Kuzmin & Natapov (1990). Between KIEV and NE53 the tectonic age of the east European platform is younger as it is influenced by the Rhiphean aulacogen (1300 Ma) and the formation of the Dnieper–Donetz depression (340 Ma); see Zonenshain, Kuzmin & Natapov (1990). Below the EEP we find a continuous high S velocity anomaly to a depth of 200 km. The seismic velocities under the Archaean Baltic shield (NE51–KEV) are slightly smaller than for the younger EEP but the anomaly extends to the same depth of 200 km. At depths larger than 300 km, the EEP shows low S velocities. A similar pattern of high velocities in the lithosphere and low velocities in the upper mantle below it has also been observed west of our profile under the EEP by Zielhuis & Nolet (1994) and Marquering & Snieder (1996). Nolet & Zielhuis (1994) relate these low velocities to the injection of water by ancient subduction along the Tornquist–Teisseyre zone. Our study confirms that in eastern Europe the geological boundary between the Proterozoic and Archaean terranes and the surrounding tectonically younger regions extends at least down to 200 km depth.

The velocities in the crustal layer of the model correlate well with the lithospheric velocities. The crustal velocities are not strongly affected by smoothing, which can been seen by the low crustal velocity under the centre of the east European platform. This anomaly can be interpreted as an image of the sedimentary layers which are present on the EEP but absent on the Baltic shield. This interpretation is, however, not correct because we have already corrected the data for such a crustal structure. We should therefore observe only very small velocity perturbations in the crust. When we omit the crustal correction we get poorer waveform fits and larger SA anomalies in the lithosphere. Therefore, the most likely explanation for the crustal anomalies is that either the applied crustal model (CRUST5.1), or the computation of the crustal correction by summing the local phase velocities in each $5^\circ \times 5^\circ$ cell, is not adequate.

There is no clear pattern in the apparent anisotropy SA under the continent. On average $SA < 1.5$ per cent and in the Barents Sea region SA is almost zero. As we already noted, SA is affected by the crustal model and we expect that further improvement of the crustal model could reduce SA. On the other hand, anisotropy is often observed under continents. For instance, an azimuthal dependence of phase velocities is observed in central Europe studies by Yanovskaya *et al.* (1990). Another indication for continental anisotropy is *SKS* splitting, which has been observed at several stations in the region (e.g. ANTO in Turkey and OBN in Russia); see Silver (1996). It is interesting to note that for station KEV, which is located on the boundary with the cell with the lowest SA value, no splitting has been observed (Silver 1996).

7 SEISMIC VELOCITIES AND TECTONIC AGE

For oceanic plates several square root and logarithmic relations between geophysical observables and the age of the ocean floor have been suggested (Sclater *et al.* 1980). The square root relation has been explained by a thermal model of a cooling half-space and is valid for oceanic lithosphere younger than 80 Ma; see Davis & Lister (1974). For older oceanic lithosphere logarithmic relations have been suggested which were explained by a model of a cooling plate laying on a half-space; see Sclater *et al.* (1980) and more recently Stein & Stein (1992). Similar relations have been proposed for continental regions. Meissner (1986) described an empirical logarithmic relation between the crustal thickness and the lithospheric age. For the Eurasian continent, Pavlenkova (1996) has shown that heat flow and P_n velocities decrease with lithospheric age. Because of the geodynamical implication of these relations we have investigated whether such a relation exists in our model.

The thickness of the continental lithosphere would be a useful parameter for such an investigation. We define the thickness of the continental lithosphere by the zero contour. In the S velocity model we see that it correlates well with the regional tectonics. Young lithosphere such as that present in the eastern Mediterranean is characterized by a very thin high-velocity lid. The thickness of this lid increases to 100 km in continental regions such as the Black Sea and Barents Sea. The high-velocity layer has a thickness of 200 km under the east European platform and Baltic. This high-velocity layer reaches its largest depth extent under the Ukrainian shield and the southern part of the EEP. The definition of the base of the lithosphere however is somehow arbitrary as it depends on which contour level has been chosen in the seismic model.

The average velocity of the lithosphere in our model is probably better resolved than the base of the lithosphere. We have computed the average S velocity perturbation between the Moho and 200 km depth. The crust is not included as a crustal correction has already been applied. The maximum depth of the integration is set to 200 km which seems to be the base of the lithosphere in our model. An uncertainty of 0.5 per cent in the average velocity has been given to each value representing the uncertainty in the model and the integration depth. The tectonic age of each has been computed using ages given by Zonenshain *et al.* (1990). Several cells have a significant uncertainty in age as tectonic blocks with different ages are sampled (e.g. KIEV–NE53). The data have been plotted on a logarithmic scale following the trend; see Fig. 7.

A least squares fit to the data is computed for both a logarithmic and a square root relation between seismic velocity and age. The quality of the fit is measured by χ^2 and should be around 1 for a good fit. The measurement for the eastern Mediterranean, indicated by the triangle in Fig. 7, has been excluded from the fit because of our conclusion that this is not a continental region. The solid line in Fig. 7 represents the fit for a logarithmic relation with $\chi^2 = 0.9$. The dashed, curved line in Fig. 7 is the fit for a square-root-of-age relation of the seismic velocities and age. The fit with the data is slightly worse with $\chi^2 = 1.2$. When the measurement for the eastern Mediterranean is included in the fitting procedure we get $\chi^2 = 0.9$ for the logarithmic relation and $\chi^2 = 2.2$ for the square root relation. These numbers support the logarithmic relation between seismic velocities and lithospheric age. However, because of

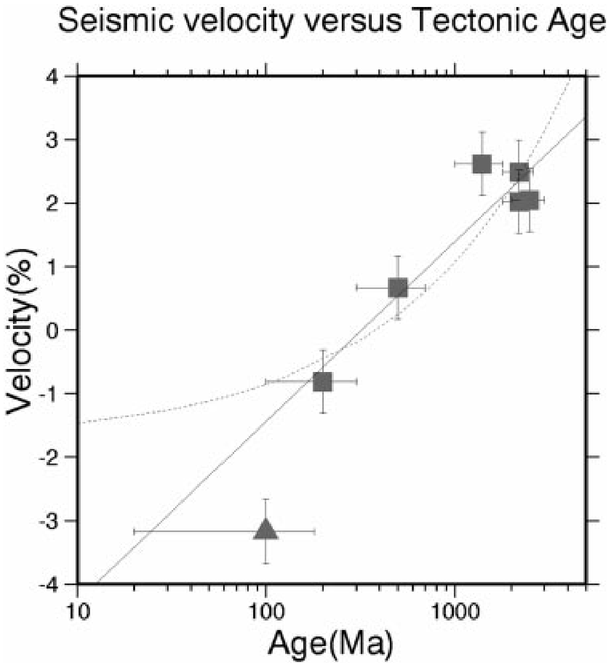

Figure 7. Seismic velocities versus tectonic age. The solid line represents a fit to the points indicated by the squares assuming a logarithmic relation. The dashed line is computed for a square root relation. The measurement for the eastern Mediterranean indicated by the triangle has been excluded from the calculation.

the uncertainties in the eastern Mediterranean and the small differences in χ^2 when this region is excluded, we conclude that our model has only a small preference for a logarithmic relation between seismic velocity and tectonic age.

8 CONCLUSIONS

Low shear velocities and strong apparent anisotropy are observed in the eastern Mediterranean. The large difference of 7 per cent in *SH* and *SV* velocities is interpreted as anisotropy. This interpretation is consistent with tectonic reconstructions of the region that predict the presence of an oceanic lithosphere. The model constructed shows the European continent as a pronounced high-velocity body extending to 200 km depth under the Proterozoic east European platform and the Archaean Ukrainian and Baltic shields. In younger continental regions such as the Black Sea and Barents Sea the high-velocity lid is thinner and extends only to a depth of 100 km. The average seismic velocities in the continental lithosphere to 200 km depth increase with tectonic age and favour a logarithmic relation. However a possible square root of age relation cannot yet be excluded. In the continent only weak apparent seismic anisotropy is observed.

ACKNOWLEDGMENTS

We would like to thank Arie van Wettum and the partners in the NARS-DEEP project for their assistance. We would also like to thank Paul Meijer for discussions and Gaby Laske for sending us the crustal model CRUST5.1. We thank the reviewers, Rob van der Hilst and Brian Mitchel, whose comments improved the manuscript. Data used in this study were made available by IRIS and GEOFON. The NARS-DEEP project is supported by the Netherlands Geoscience Foundation (GOA) through grant 751.360.001 and through INTAS project 93-1076. This work was conducted under the programme of the Dutch national research school, the Vening Menesz Research School of Geodynamics.

REFERENCES

Babuska, V. & Cara, M., 1991. *Seismic Anisotropy in the Earth,* Kluwer Academic, Dordrecht.

Cloetingh, S., Nolet, G., & Wortel, R., 1980. Crustal structure of the eastern Mediterranean inferred from Rayleigh wave dispersion, *Earth planet. Sci. Lett.,* **51,** 336–342.

Davis, E.E & Lister, C.R.B., 1974. Fundamentals of ridge crest topography, *Earth planet. Sci. Lett.,* **21,** 405–413.

Dercourt, J. *et al.*, 1986. Geological evolution of the Tethys from the Atlantic to the Pamirs since the Lias, *Tectonophysics,* **123,** 241–315.

Durrheim, R.J., & Mooney, W.D., 1994. Evolution of Precambrian lithosphere: seismological and geochemical constraints, *J. geophys. Res.,* **99,** 15 359–15 374.

Dziewonski, A.M. & Anderson, D.L., 1981. Preliminary Reference Earth Model, *Phys. Earth planet. Inter.,* **25,** 297–356.

Grad, M., Kryzanowska, M. & Pirhonen, S.E., 1995. Inhomogeneities of the Eurasian mantle structure from the traveltimes of the nuclear explosions recorded by the Finnish seismic network during 1961–1985, *Geophys. J. Int.,* **121,** 863–872.

Jordan, T.H., 1981. Continents as a chemical boundary layer, *Phil. Trans. R. Soc. Lond.* A, **301,** 359–373.

Husebye, E.S., & Hovland, J., 1982. On upper mantle seismic heterogeneities beneath Fennoscandia, *Tectonophysics,* **90,** 1–17.

Levshin, A. & Ratnikova, L., 1984. Apparent anisotropy in inhomogeneous media, *Geophys. J. R. astr. Soc.,* **76,** 65–69.

Marquering, H. & Snieder, R., 1996. Shear wave velocity structure beneath Europe, eastern Atlantic and western Asia from waveform inversions including mode coupling, *Geophys. J. Int.,* **127,** 283–304.

Meissner, R., 1986. *The Continental Crust: A Geophysical Approach,* Academic Press, San Diego, CA.

Mitchel, B.J., 1984. On the inversion of Love- and Rayleigh-wave dispersion and implications for Earth structure and anisotropy, *Geophys. J. R. astr. Soc.,* **76,** 233–241.

Mooney, W.D., Laske, G. & Masters, G., 1998. CRUST5.1: A global crustal model at 5 × 5 degrees, *J. geophys. Res.,* **103,** 727–747.

Muyzert, E.J. & Snieder, R.K., 1996. The influence of errors in the source parameters on phase velocity measurements of surface waves, *Bull. seism. Soc. Am.,* **86,** 1863–1872.

Nishimura, C.L. & Forsyth, D.W., 1989. The anisotropic structure of the upper mantle in the Pacific, *Geophys. J. Int.,* **96,** 203–229.

Nolet, G., 1990. Partitioned waveform inversion and the two-dimensional structure under the network of autonomously recording seismographs, *J. geophys. Res.,* **95,** 8499–8512.

Nolet, G. & Zielhuis, A., 1994. Low *S* velocities under the Tornquist–Teisseyre zone: Evidence for water injection into the transition zone by subduction, *J. geophys. Res.,* **99,** 15 813–15 820.

Paige, C.C. & Saunders, M.A., 1982. LSQR: an algorithm for sparse linear equations and sparse least squares, *ACM Trans. Math. Soft.,* **8,** 195–209.

Pavlenkova, N.I, 1996. Crust and upper mantle structure in northern Eurasia from seismic data, *Adv. Geophys.,* **37,** 1–121.

Snieder, R. & Paulssen, H., 1993. Future deployment of the NARS array, *Proc. Europrobe Symp.,* 129–132, Jablonna, 1991.

Sclater, J.G., Jaupert, C. & Galson, D., 1980. The heat flow through oceanic and continental crust and the heat loss of the earth, *Rev. Geophys. Space Phys.,* **18,** 269–311.

Silver, P.G., 1996. Seismic anisotropy beneath the continents: Probing the depths of geology, *Ann. Rev. Earth planet. Sci.,* **24,** 385–432.

Stein, C.A. & Stein, S., 1992. A model for the global variation in oceanic depth and heat flow with lithospheric age, *Nature,* **359,** 123–129.

de Voogd, B., Truffert, C., Chamot-Rooke, N., Huchon, P., Lallemant, S. & le Pichon, X., 1992. Two-ship deep seismic soundings in the basins of the eastern Mediterranean Sea (Pasiphae cruise), *Geophys. J. Int.,* **109,** 536–552.

Yanovskaya, T.B., Panza, G.F., Ditmar, P D., Suhadolc, P. & Mueller, S., 1990. Structural heterogeneity and anisotropy based on 2-D phase velocity patterns of Rayleigh waves in western Europe, *Atti dell Acca. Naz. dei Lincei Rendiconti,* **9,** 127–135.

Zielhuis, A. & Nolet, G., 1994. The deep seismic expression of an ancient plate boundary in Europe, *Science,* **265,** 79–81.

Zonenshain, L.P., Kuzmin, M.I. & Natapov, L.M., 1990. Geology of the USSR: A plate tectonic synthesis, *Geodynam. Series,* **21,** *Am. geophys. Un. Monogr.*